Dynamic Converter Capacity Allocation for Multifunctional Energy Storage Systems in Oil and Gas Applications

Spyridon Chapaloglou
Dept. of Electric Power Engineering
Norwegian University of Science and Technology (NTNU)
Trondheim, Norway
spyridon.chapaloglou@ntnu.no

Danilo I. Brandao
Dept. of Electrical Engineering
Federal University of Minas Gerais (UFMG)
Belo Horizonte, Brazil
dibrandao@ufmg.br

Elisabetta Tedeschi
Dept. of Electric Power Engineering
Norwegian University of Science and Technology (NTNU)
Trondheim, Norway and
Dept. of Industrial Engineering
University of Trento, Italy
elisabetta.tedeschi@ntnu.no

***Abstract*—In this paper, a power management strategy is proposed for enhancing the benefits of energy storage systems to wind powered offshore Oil and Gas platforms. Different functionalities of the converter, such as following a charging schedule from an upper layer control and active power filtering are dynamically assessed, and the converter capacity is optimally allocated among the different services, while preserving the stability of the converter-controllers interactions. To achieve that, a non-linear controller is developed, allowing for full range regulation of the energy storage. To demonstrate the proposed power management strategy, a dynamic model of a platform section is developed and time domain simulations are carried out. The results revealed that load generated reactive, harmonic and unbalanced currents could be successfully compensated, improving the local power quality indices while following the storage charging schedule and respecting the converter limitations under both static and transient conditions, so that the converter cost-benefit relation is improved.**

***Index Terms*—Oil and Gas (O&G), offshore platforms, power quality, battery energy storage, conservative power theory**

I. Introduction

The recent technological improvements in RES efficiency, and the price reduction trend of batteries storage systems, have captured the interest of the Oil and Gas (O&G) industry. These two points come in hand for the offshore installations that need to adapt to the strict environmental regulations through hybrid power plants concepts [1]. The high renewable potential of such offshore locations is considered as an alternative to the costly and infrastructure-demanding power from shore concept. Different types of RES have been studied for integration to offshore platforms [2], with wind being a promising solution [3], [4]. However, the task of integrating such intermittent energy sources in isolated platform grids characterized by large and dynamic loads [5], can be benefited from the support of energy storage in several ways. In particular, studies have shown that integrating appropriately sized battery energy storage systems (BESS) to O&G applications can contribute to increased reliability [6], fuel efficiency improvements [7] and operating costs reduction [8]. In [9], the added value of energy storage in terms of enhancing frequency and voltage stability of a platform's power system, was reported, whereas in [10], [11] the particular technology of Li-ion batteries was proposed for reducing the transient load power deviation.

Large inductive loads typically found in O&G platforms are associated with the need for bulky passive components for reactive compensation, while the Variable Frequency Drives (VFD) can be particularly hazardous for weak power systems as their effects (i.e. voltage sags and distortion) can propagate, affecting sensitive loads [12]. In [13] a series active power filter was proposed to mitigate problems related to harmonic current from VFDs and source voltage unbalance. However, as such solutions usually require large scale power converters interconnected to MV levels, more complex converter topologies may be required to keep the efficiency high [14]. Alternatively, the use of converters based on wide band-gap semiconductors can be considered [15].

As it is evident from the above-mentioned analysis, the benefits coming from i) BESS and ii) APF integration to O&G platforms have been separately addressed aiming for different types of support. Nevertheless, both of them could be combined and offered simultaneously through an appropriate system design and control scheme using the concept of multi-functional converters [16]. This can be facilitated through the use of the Conservative Power Theory (CPT) which decomposes the current and power of a single or multi-phase system [17] into orthogonal components having a precise physical meaning. The effects of such components can then be addressed individually. However, providing many services simultaneously can bring to surface issues coming from the interaction of different control loops of the interconnected subsystems (i.e. DC and AC side), whose design is often decoupled. For that, an appropriate power management strategy capable of dealing with these interactions is proposed in this paper, which provides the combined BESS/APF services without requiring converter oversizing. The rest of the paper is organized as follows: In section II the equivalent model of

the platform is derived, in section III the power management system design is presented, in section IV the simulation results are analyzed and finally in section V the main conclusions are discussed.

II. System Modeling and Design

The model developed in this paper represents a simplified version of an existing offshore installation. Since the complete platform power system is rather complex and would not necessarily bring further insights into the paper subject, a simplification is made by detailing a part of the whole system and representing the unmodeled part (shaded region in fig. 1) like an equivalent voltage source, without AVR and governor controllers.

A. Platform power system description

The complete platform power system is illustrated in fig. 1. As it is possible to note, the power generated from two identical synchronous generators (SG) at the specified "medium voltage 1" level (MV1) is transferred to the MV1 bus to supply local MV1 loads, and to the "medium voltage 2" level (MV2) through a step down transformer. The MV2 bus is then connected to some MV2 loads and another step down transformer that supplies the "low voltage" (LV) loads of the platform, including the living-quarter loads and the power converter of the interconnected BESS. The parameter values for the complete system are presented in table I. For

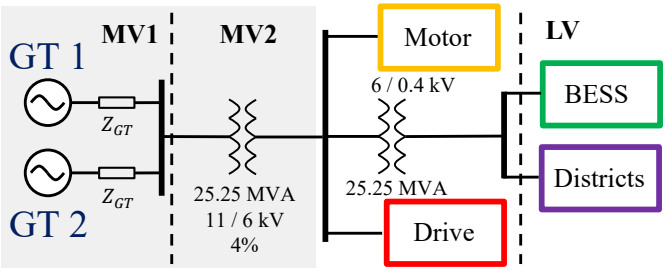

Fig. 1. Platform power system.

TABLE I
Platform Power Grid Parameters

Parameter	Symbol	Value	Units
SG Power rating	S_{GT}	25.25	[MVA]
SG Nominal Voltage (line-line)	$V_{nom,HV}$	11	[kV]
SG Subtransient Reactance	X''_d	24	[%]
HV Transformer power rating	S_{TF}	25.25	[MVA]
HV Transformer ratio	N_{TF}	11/6	[-]
HV Transformer SC impedance	Z_{TF}	4	[%]
Nominal frequency	f_g	60	[Hz]
Source short-circuit level	S_{sc}	157.8	[MVA]
Source short-circuit impedance	z_{sc}	0.16	[pu]
Source inductance	L_g	0.6021	[mH]
Source resistance	R_g	0.0227	[Ohms]

the simulations purposes, the part of the platform until the MV was replaced by a voltage source behind an equivalent short-circuit impedance and a calculated short-circuit (SC) capability at the specified point of common coupling (PCC). The rest of the system was modeled in detail, as it is possible to see from fig. 2. In this figure, an equivalent 3-phase 3-wire system with grounded neutral, interconnecting three main loads (representing three different types of loads typically met in a platform) is illustrated. The induction motors (i.e. water/mud pumps [7]) were modeled by an equivalent direct-on-line linear load (subscript rl) and a constant power factor, the DC drives (i.e. draw-works VFD) by an equivalent non-linear load (subscript nl) composed of a full bridge, naturally commutated 3-phase rectifier, and a series connected inductor-resistor at the dc side and finally, the residential districts (i.e. single phase low voltage loads) by an equivalent resistive unbalanced load (subscript ul). In addition, at the LV side it is possible to observe the power electronic interface of the BESS. It is composed of a 2-level 3-phase voltage-source converter connected to the 6 kV through a 400 V to 6 kV transformer, responsible for the power exchange between the AC and DC side, and a half-bridge bidirectional DC/DC boost converter (synchronous rectification) connecting the DC link with the BESS. The parameters associated to the detailed model are presented in table II.

TABLE II
Load Parameters

Parameter	Symbol	Value	Units
Linear load (rl) nominal power	S_{rl}	1	[MVA]
rl nominal voltage (line-line)	$V_{nom,MV}$	6	[kV]
rl power factor	PF_{rl}	0.89	[-]
Non-linear load (nl) inductance	L_{nl}	0.1306	[H]
Non-linear load (nl) resistance	R_{nl}	96.1200	[Ohms]
Unbalance load (ul) nominal power	P_{ul}	0.5	[MW]
ul nominal voltage (line-line)	$V_{nom,LV}$	0.4	[kV]

B. Detailed representation of MV/LV section

To estimate the source inductance and resistance from the input short circuit impedance, a ratio of $X/R = 10$ was assumed [16] [15]. The source parameters are presented in table I. A sinusoidal PWM modulation scheme is used for the AC/DC converter and an LC output filter is designed (assuming a maximum current ripple 20%) as in [18]

$$L_f = \frac{V_{dc}}{6 f_s \Delta I_{L,max}},\ C_f = \frac{1}{4\pi^2 L_f f_{res}^2} \tag{1}$$

The symbols in eq. (1) are defined later in table III. Lastly, a small series connected parasitic resistance and a damping resistor [19] are considered in series with the L_f and C_f respectively. The converter's parameters are presented in table III. The converter's output apparent power is given as

$$S_o = \mathbf{V_o^c I_o^c} = \|\vec{v}_o\|\|\vec{i}_o\| = \sqrt{\sum_n^{A,B,C}\left(\frac{1}{T}\int_0^T v_{o,n}^2\,dt\right)}\sqrt{\sum_n^{A,B,C}\left(\frac{1}{T}\int_0^T i_{o,n}^2\,dt\right)} \tag{2}$$

where $\mathbf{V_o^c}$, $\mathbf{I_o^c}$ are the collective rms voltage and current values, $v_{o,n}$, $i_{o,n}$ the virtual star phase voltage and current measurements at the converter output and T the averaging period for

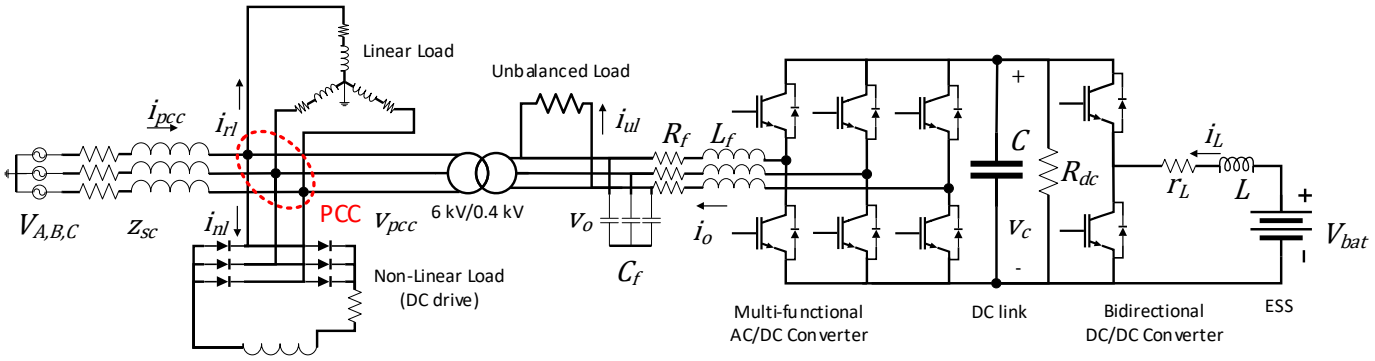

Fig. 2. Detailed simulation model of the O&G platform.

TABLE III
POWER CONVERTERS PARAMETERS

Parameter	Symbol	Value	Units
DC link voltage	V_{dc}	750	[V]
DC link capacitor	C	8.296	[mF]
DC/DC switching frequency	$f_{s,dc}$	10	[kHz]
DC/DC design current	I	2500	[A]
DC load	R_{dc}	10	[Ohms]
Battery Nominal voltage	V_{bat}	400	[V]
DC filter inductor	L	0.747	[mH]
DC filter parasitic resistance	r_L	0.01	[Ohms]
Design Duty Ratio	D	0.4667	[-]
DC/AC nominal power	S_r	1	[MVA]
DC/AC base current	I_{inv}	2000	[A]
DC/AC switching frequency	$f_{s,inv}$	9720	[Hz]
DC/AC resonance frequency	f_{res}	4000	[Hz]
DC/AC filter inductance	L_f	0.0445	[mH]
DC/AC filter capacitance	C_f	35.5374	[μF]
DC/AC filter resistance	R_f	0.0100	[Ohms]

calculating the rms values of the signals, corresponding to the inverse of the grid frequency, $f_g = 60\ Hz$. Using CPT and the current decomposition into active i_a , (balanced) reactive i_r^b, void i_v (responsible for current distortion) and unbalance i_u components eq. (2) can be rewritten as

$$S_o = \sqrt{P_o^2 + Q_o^2 + D_o^2 + N_o^2} \tag{3}$$

where P_o, Q_o, D_o, N_o stand for the active, reactive, distortion and unbalance power components of the converter, respectively. Those are calculated following [20] as

$$P_o = \frac{1}{T} \sum_n^{A,B,C} \left(\int_0^T v_{o,n} i_{o,n}\, dt \right) \tag{4}$$

$$Q_o = \frac{1}{T} \sum_n^{A,B,C} \left(\int_0^T \hat{v}_{o,n} i_{o,n}\, dt \right) \tag{5}$$

where $\hat{v}(t)$ represents the unbiased integral of $v(t)$ times the grid angular frequency $\omega = 2\pi f_g$.

$$\left|D_o\right| = \|\vec{v}_{pcc}\| \|\vec{i}_{nl,v}\| \ \text{ where, } \vec{i}_{nl,v} = \vec{i}_{nl} - \vec{i}^{\,b}_{nl,\mathrm{a}} - \vec{i}^{\,b}_{nl,r} \tag{6}$$

$$\vec{i}^{\,b}_{nl,\mathrm{a}} = \frac{\sum_n^{A,B,C} \left(\frac{1}{T} \int_0^T v_{pcc,n} i_{nl,n}\, dt \right)}{\|\vec{v}_{pcc}\|^2} \vec{v}_{pcc} \tag{7}$$

$$\vec{i}^{\,b}_{nl,r} = \frac{\sum_n^{A,B,C} \left(\frac{1}{T} \int_0^T \hat{v}_{pcc,n} i_{nl,n}\, dt \right)}{\|\vec{\hat{v}}_{pcc}\|^2} \vec{\hat{v}}_{pcc} \tag{8}$$

$$\left|N_o\right| = \|\vec{v}_o\| \|\vec{i}_{ul,u}\| \ \text{ where, } \vec{i}_{ul,u} = \vec{i}^{\,u}_{ul,\mathrm{a}} + \vec{i}^{\,u}_{ul,r} \text{ where,}$$

$$\vec{i}^{\,u}_{ul,\mathrm{a}} = \begin{bmatrix} \frac{\int_0^T v_{o,A} i_{ul,A}\, dt}{\int_0^T v_{o,A}^2\, dt} v_{o,A} \\ \frac{\int_0^T v_{o,B} i_{ul,B}\, dt}{\int_0^T v_{o,B}^2\, dt} v_{o,B} \\ \frac{\int_0^T v_{o,C} i_{ul,C}\, dt}{\int_0^T v_{o,C}^2\, dt} v_{o,C} \end{bmatrix} - \frac{\sum_n^{A,B,C} \left(\frac{1}{T} \int_0^T v_{o,n} i_{ul,n}\, dt \right)}{\|\vec{v}_o\|^2} \vec{v}_o,$$

$$\vec{i}^{\,u}_{ul,r} = \begin{bmatrix} \frac{\int_0^T \hat{v}_{o,A} i_{ul,A}\, dt}{\int_0^T \hat{v}_{o,A}^2\, dt} \hat{v}_{o,A} \\ \frac{\int_0^T \hat{v}_{o,B} i_{ul,B}\, dt}{\int_0^T \hat{v}_{o,B}^2\, dt} \hat{v}_{o,B} \\ \frac{\int_0^T \hat{v}_{o,C} i_{ul,C}\, dt}{\int_0^T \hat{v}_{o,C}^2\, dt} \hat{v}_{o,C} \end{bmatrix} - \frac{\sum_n^{A,B,C} \left(\frac{1}{T} \int_0^T \hat{v}_{o,n} i_{ul,n}\, dt \right)}{\|\vec{\hat{v}}_o\|^2} \vec{\hat{v}}_o \tag{9}$$

In eqs. (2), (4) and (5) n represents the phase index. The linear, non linear and unbalanced loads are indexed by rl, nl, ul respectively.

C. Bidirectional DC/DC converter modelling

The BESS is considered to be composed of several strings of series connected Li-ion cells to reach the rated voltage and power [21] and connected to the rest of the grid through a bidirectional DC/DC converter, providing constant voltage at the DC link. Even though this could be achieved with the inverter itself through a secondary outer loop, this would result in an additional active current component that could interact with the active current reference commanded from the active power tracking operation. Therefore, this task was assigned to the bidirectional DC/DC buck-boost converter interfacing the battery storage with the rest of the grid. Even though a non-linear switching model was used for the modeling of this converter, the basic behavior can be explained through the following averaged equations

$$\begin{bmatrix} \dot{i}_L \\ \dot{v}_C \end{bmatrix} = \begin{bmatrix} \frac{-r_L}{L} & -\frac{(1-d_v)}{L} \\ \frac{(1-d_v)}{C} & -\frac{1}{R_{dc}C} \end{bmatrix} \begin{bmatrix} i_L \\ v_C \end{bmatrix} + \begin{bmatrix} \frac{1}{L} & 0 \\ 0 & -\frac{1}{C} \end{bmatrix} \begin{bmatrix} V_{bat} \\ i_z \end{bmatrix} \tag{10}$$

where r_L is the filter parasitic resistance, R_{dc} models a linear DC load, i_z the load current source modelling the power demand from the DC side of the DC/AC converter and d_v the

control input duty cycle and V_{bat} the battery input voltage. The filter inductance and output capacitance were calculated for a specified design point of the converter with $i_L = \bar{I}$ and $d_v = D$, assuming a current ripple coefficient $\delta = 1\%$ and following the equations

$$L = \frac{D(1-D)^2\bar{I}}{V_{bat}\delta f_{s,dc}},\ C = \frac{V_{bat}D}{\bar{I}\delta f_{s,dc}} \tag{11}$$

The converter's parameter values are presented in table III.

III. Power Management and Control Design

An overview of the proposed power management and control algorithm is presented in fig. 3. In this figure the proposed hierarchical nested structure is depicted, with the DC/AC converter's current controller and the DC/DC converter's voltage controller receiving their set-points from the outer layer power loop, implementing the dynamic converter capacity allocation strategy. The compensation goal is to achieve unity power factor at the PCC by using the energy storage converter.

A. DC/AC converter as controlled current source

For the current control loop of the DC/AC converter, 2 PI controllers are designed in the *abc* frame, giving the current reference for the two phases while the third was derived as the negative sum of the two other [22]. The design procedure followed was based on [23]. The reference current is calculated based on the CPT theory due to its inherent capability to separate the effects of different phenomena, associated possibly with different elements of the grid. Therefore, the current reference is generated from a combination of decomposed references as follows: the active current reference was determined from the active power command P^* and either resistive load synthesis (RLS) (using the measured output voltage) or sinusoidal current injection (SCI) (using the fundamental component of the voltage waveform). As it was proved in [16] when the active command is related to power absorption (charging the BESS) the RLS is better suited, providing extra damping to the source, whereas for power injections (BESS discharging) the SCI is preferable, usually associated with lower level of harmonics injection. The two methodologies were implemented through eq. (12).

$$\vec{i}_{\mathrm{a}}^{*} = \begin{cases} \frac{P^*}{\|\vec{v}_o\|^2}\vec{v}_o, & \text{charging, } P^* < 0 \\ \frac{P^*}{\|\vec{v}_o\|^2}\vec{v}_{o,1}, & \text{discharging, } P^* > 0 \end{cases} \tag{12}$$

where, $\vec{v}_{o,1}$ is the 3-phase fundamental voltages. The non-linear load generates harmonic current while both the former and the liner load are associated mainly with a reactive power consumption. The current references to compensate for reactive, harmonic and unbalanced currents are given as

$$\begin{aligned} \vec{i}_r^{\,b^*} &= \frac{-(Q_{rl}+Q_{nl})}{\|\vec{\hat{v}}_{pcc}\|^2}\vec{\hat{v}}_{pcc} \ \text{ where,} \\ Q_{rl} &= \sum_n^{A,B,C}\left(\frac{1}{T}\int_0^T \hat{v}_{pcc,n} i_{rl,n}\,dt\right) \\ Q_{nl} &= \sum_n^{A,B,C}\left(\frac{1}{T}\int_0^T \hat{v}_{pcc,n} i_{nl,n}\,dt\right) \end{aligned} \tag{13}$$

$$\vec{i}_v^{\,*} = -\vec{i}_{nl,v} \tag{14}$$

$$\vec{i}_u^{\,*} = -\vec{i}_{ul,u} \tag{15}$$

respectively. Finally, the control input to the converter can be expressed as

$$\begin{gathered} \vec{d}_i^{\,*} = \left(K_{P,i} + \frac{K_{I,i}}{s}\right)\left(\vec{i}^{\,*} - \vec{i}_o\right), \text{ where,} \\ \vec{i}^{\,*} = \vec{i}_{\mathrm{a}}^{\,*} + \vec{i}_r^{\,b^*} + \vec{i}_v^{\,*} + \vec{i}_u^{\,*} \end{gathered} \tag{16}$$

B. DC/DC converter as controlled voltage source

When it comes to energy storage components, where the operating conditions change considerably, designing a controller for the highly non-linear system eq. (10) is not a trivial task. In this study a non-linear controller was designed for the full operating range of the storage system based on the gain scheduling technique, which is commonly used in practice. For each operating point, the following procedure was followed. The small signal linearized version of the system eq. (10) was considered as

$$\begin{bmatrix} \dot{\tilde{i}}_L \\ \dot{\tilde{v}}_C \end{bmatrix} = \begin{bmatrix} \frac{-r_L}{L} & -\frac{(1-D)}{L} \\ \frac{(1-D)}{C} & -\frac{1}{RC} \end{bmatrix}\begin{bmatrix} \tilde{i}_L \\ \tilde{v}_C \end{bmatrix} + \begin{bmatrix} \frac{V_{ss}}{L} \\ -\frac{I_{ss}}{C} \end{bmatrix}\tilde{d}_v + \begin{bmatrix} 0 \\ -\frac{1}{C} \end{bmatrix}\tilde{i}_z \tag{17}$$

where V_{ss}, I_{ss} are the equilibrium values at each specified operating point defined from the DC value of the load current I_z. Then, an optimal local linear controller was designed based on the LQR methodology and an outer integrator (as depicted in fig. 3 resulting in the following control structure

$$d_v^* = -\left(K_L\left(i_L - I_{ss}\right) + K_C\left(v_C - V_{ss}\right)\right) - \left(\frac{K_{v,i}}{s}\left(v_C - V_{dc}\right)\right) \tag{18}$$

where the state's measurements where first low pass filtered. The scheduling variable which represented the load current at the DC side of the DC/AC converter was estimated as $\frac{P^*}{V_{dc}}$, linking the outer power loop with the DC link voltage control. Finally, the parameters $K_L, K_C, V_{ss}, I_{ss}, K_{v,i}$ were calculated for the different operating points and a linearly interpolated map was used to continuously vary them.

C. Dynamic capacity allocation

Even though the developed control system in section III is capable of dealing efficiently around different operating points, its good performance is not guaranteed for the transition from one point to another, under all circumstances. This effect becomes clear when such variations are of large magnitude and at the same time the converter has to provide the additional grid services (i.e. compensation as described in section III-A). We explicitly state that in our system, power quality improvement was prioritized, considering the potential deterioration that could arise from significant load transients and even the possible interconnection of wind farms on the upper level grid, which is in line with the trends described in section I. In addition we assume a load following operation of the BESS, where the large load variations of the upper level grid (i.e. due to large motor disconnections) are directly reflected to the

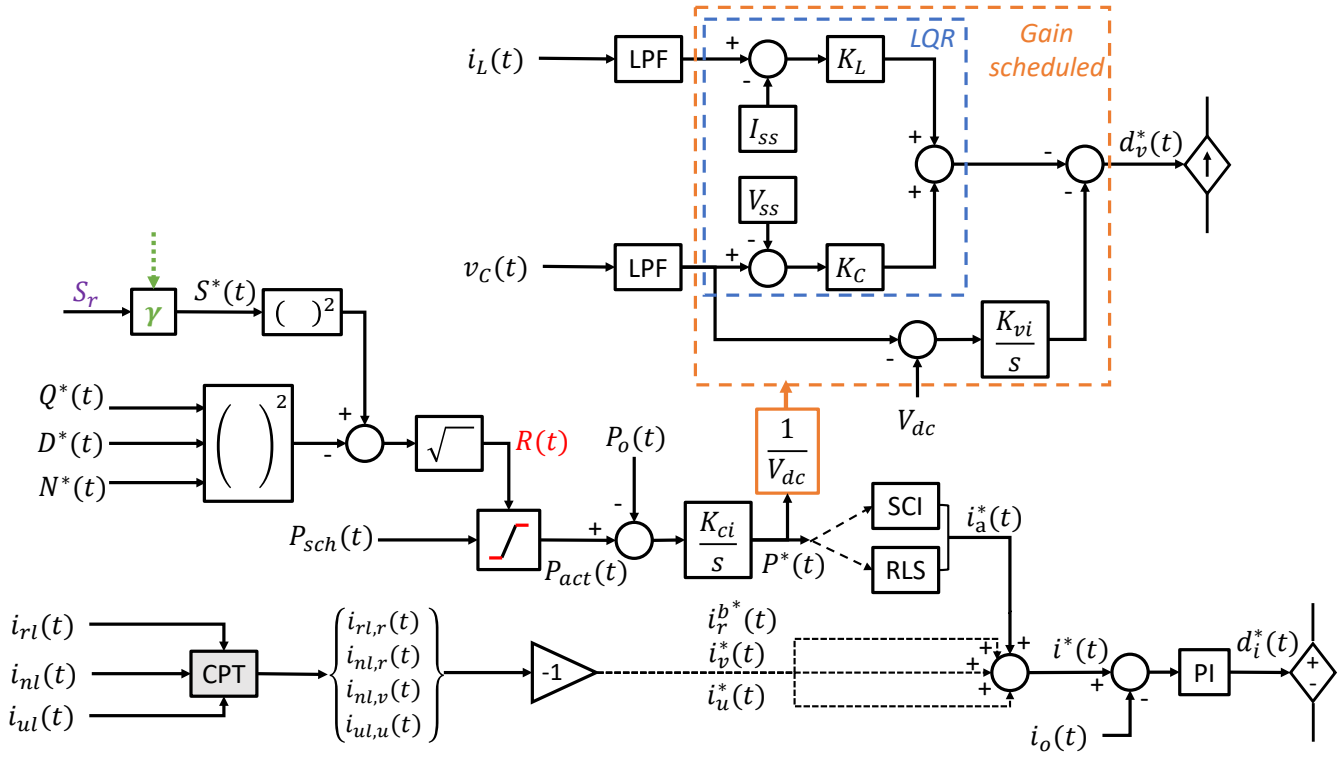

Fig. 3. Proposed power management and control strategy.

active power scheduling command and require an immediate (large signal) response from the BESS. If these conditions are replicated in the simulations of the high-fidelity non-linear model (fig. 2) which includes the interactions of the control loops of the different subsystems, then power overshoots that violate the converter's limits (i.e. $S_o(t) > S_r$) may be noticed during transients.

To deal with this problem, in this paper we propose a power management strategy that sets feed-forward dynamic limits on the active power reference, based on prior information of the disturbances to come (i.e. charge/discharge schedule and load connections/disconnections). In this way, we can guarantee that the output converter power $S_o(t) \leq S_r$ under all anticipated disturbances. To do that, we rely on a high fidelity simulation model (fig. 2) of the actual plant, serving as its digital twin to predict such disturbances. This assumption could be considered not far from reality, since for O&G applications, typically the loads and BESS schedules could be provided in advance from an upper layer energy management system (EMS).

In the proposed power management strategy, the dynamic grid services (compensation) provision are considered and prioritized over small deviations from the active power schedule. Therefore, at each instant the converter can afford a theoretical maximum active power provision defined as

$$\left|P_{act}^{max}\right| \leq \sqrt{S_r^2 - Q^{*2} - D^{*2} - N^{*2}} \tag{19}$$

However, even though this condition can protect the converter from an infeasible combination of BESS schedule and compensation during static conditions, it does not during transient. For that purpose, we further restrict the active power command by introducing a dynamic coefficient $\gamma(t)$ allocating (reserving) some converter capacity as a margin for the upcoming overshoots. This strategy is implemented through the following equations.

$$S^* = \gamma(t) S_r \tag{20}$$

$$R(t) = \sqrt{S^{*2} - Q^{*2} - D^{*2} - N^{*2}} \tag{21}$$

$$P_{act}(t) = \begin{cases} R(t), & P_{sch}(t) \geq R(t) \\ P_{sch}(t), & -R(t) < P_{sch}(t) < R(t) \\ -R(t), & P_{sch}(t) \leq -R(t) \end{cases} \tag{22}$$

$$P^*(t) = \frac{K_{ci}}{s}\left(P_{act}(t) - P_o(t)\right) \tag{23}$$

where $R(t)$ represents the maximum (residual) active power capacity that the converter can track without risking an overshoot (i.e. $S_o(t) > S_r$) and $P_{sch}(t)$ the scheduled active power command coming from the upper layer EMS for the BESS. When $\gamma(t) = 1$ condition eq. (21) degenerates to condition eq. (19). To find the appropriate $\gamma(t)$ signal which will satisfy $S_o(t) \leq S_r$ under all anticipated future disturbances, an exhaustive search is run, using the digital twin model. In that sense, we simulate the twin (fig. 2) for a particular operating

pattern (sequence of disturbances), and check whether the specified goal ($S_o(t) \leq S_r$) is achieved under all disturbances included in that pattern. Once we achieve a satisfactory $S_o(t)$ trajectory, the signal $\gamma(t)$ is fixed. A graphical illustration of the proposed strategy is also depicted in fig. 3.

Finally, the impact of each power component to the converter output is quantified through the factors $\lambda, \lambda_Q, \lambda_U, \lambda_D$ which stand for power factor, the reactivity factor, unbalance factor and distortion factors respectively, defined as

$$\lambda = \sqrt{(1-\lambda_Q^2)(1-\lambda_D^2)(1-\lambda_U^2)} = \frac{|P_o|}{S_o}$$
$$\lambda_Q = \frac{|Q_o|}{\sqrt{P_o^2+Q_o^2}},\ \lambda_U = \frac{|N_o|}{\sqrt{P_o^2+Q_o^2+N_o^2}},\ \lambda_D = \frac{|D_o|}{S_o} \tag{24}$$

IV. Simulation Results and Analysis

To demonstrate the effectiveness of the proposed control configuration and power management strategy, numerical simulations were carried out in Matlab/Simulink simulation environment. A series of events was considered to capture all relevant modes of operation. To emulate the charging schedule following capability of the BESS, an active power reference was implemented through the signal $P_{sch}(t)$, including step changes of large magnitude, to span the whole operating range.

At the beginning of the simulation, all 3 loads (rl, nl, ul) are connected and the BESS is charging with unity power factor at -0.2 pu. Thus, all the necessary reactive power, harmonic and unbalance currents are provided by the source at the PCC, as shown in fig. 4a before the green line. At *t=0.1 s* the reactive compensation is activated and the shift between the voltage and current waveforms is directly diminished (fig. 4a after the green line). This is also depicted in fig. 6 where the source reactive power Q_s goes to zero and this starts being provided by the converter. Then at *t=0.2 s* the harmonic compensation is activated and from fig. 4b we can observe that the current waveforms at the PCC become more sinusoidal, improving significantly the total demand distortion (TDD) as defined in IEEE standard-519 [24] (table IV). At *t=0.3 s* the unbalance compensation begins, and as shown in fig. 4c, the current waveforms from the PCC become balanced. Since N_o directly affects S_o, keeping the same active power P_o means that the distortion factor will also change, resulting in a small deterioration of the TDD at the PCC (table IV). From the same table we also observe that in order to provide full compensation to the PCC (unity power factor), at the specified charging level (-0.2 pu) the converter has to operate at a power factor 0.243.

Throughout the compensation period the battery is providing the required current corresponding to the charging power level $P_{act}(t)$ (fig. 5b), while the DC link is regulated to its nominal value (fig. 5c). During the unbalance compensation period ($t = 0.3 - 0.6s$) low frequency DC link voltage oscillations are revealed, originating from the oscillation on the instantaneous active power at the converter´s terminal. These can be attributed to the power recirculation among the phases

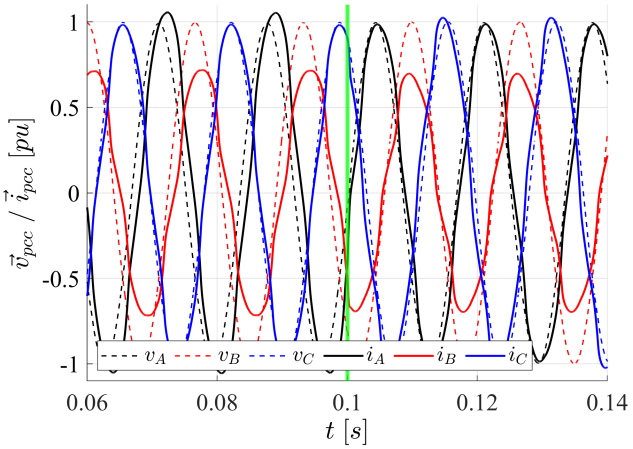

(a) Reactive compensation activated at $t = 0.1s$

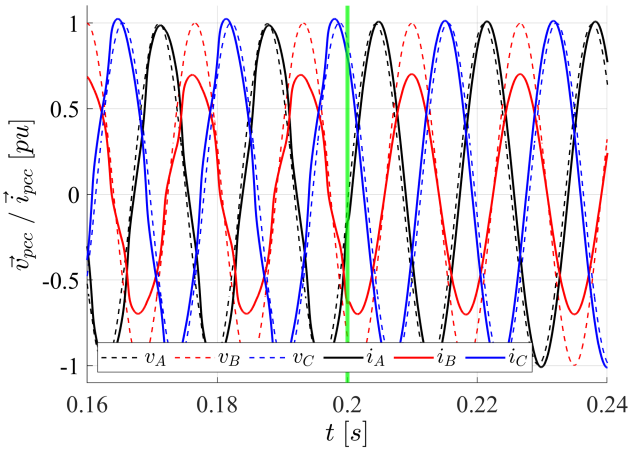

(b) Harmonics compensation activated at $t = 0.2s$

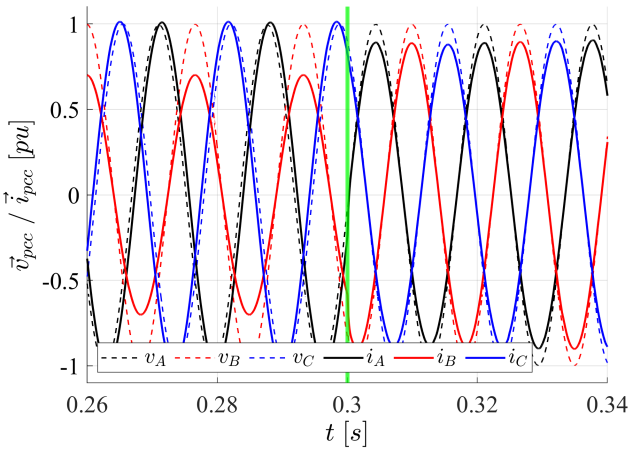

(c) Unbalance compensation activated at $t = 0.3s$

Fig. 4. Input current and voltages at the PCC before and after different compensation services are activated (green line).

at the DC/AC converter, as a consequence of providing the required unbalance power to the 3 wire AC grid. Nevertheless, the proposed DC/DC control scheme efficiently deals with those, by not allowing these oscillations to impact significantly the inductor current which would potentially lead to increased battery degradation.

Then, to demonstrate the effect of the dynamic capacity allocation algorithm, two cases including significant disturbances were simulated and compared. In the first case a constant signal $\gamma(t) = 1$ was selected (reference case), while for the second an appropriate dynamic trajectory $\gamma(t) = \gamma^*$ was defined as explained in section III-C. At *t=0.6 s* two events were realized simultaneously where the active power reference changed from -0.2 to 0.5 (BESS discharging and providing part of the active power to the local loads) and the unbalance load was disconnected. In addition, right afterwards at *t=0.7 s* the linear load was disconnected, enhancing the severity of the disturbance (less damping characteristics of the grid). The combined effect of these events resulted in oscillations of the DC link voltage (fig. 5c) and a transient variation of the converter's reactive power output, originating from the interaction of the current and voltage controllers. As can be observed from fig. 7, for such a combined disturbance to be attenuated with the given control structure, the converter's output power should go above the rated value. However, by lowering the value of $\gamma(t)$ just around the instance of the disturbance, the transient response of the converter's output remains below the rated value (fig. 7) while at the same time no steady state error is introduced, since eventually the $\gamma(t)$ value returns to unity, allowing the full use of the converter capacity S_r. The effect of lowering locally the value of $\gamma(t)$ is also depicted in the scheduling variable (fig. 5a), making the variation smoother and eventually achieving a smaller peak amplitude of the voltage oscillations (fig. 5c).

In addition, the proposed power management system is capable of dealing with variations close to the operating limits of the battery. At *t=1.1 s* a higher than before discharging power is requested from the battery, making it dominate the local grid (exporting power to source, $P_s < 0$). When $\gamma(t)$ is not compensated, for this transition to happen, not only the converter output power should again go above its rated value (fig. 7), but also power larger than the battery's power rating would be requested (fig. 5b). However, adjusting the $\gamma(t)$ signal accordingly, both limits could be respected and a decrease in the magnitude of DC link voltage oscillations was also achieved. However, in order for the battery to satisfy its limit in transient operation (fig. 5b) a steady state error was introduced to the DC/AC converter's active power output. Finally, the same effects of selecting appropriate $\gamma(t)$ trajectory was demonstrated for a large active power variation at *t=1.5 s*, where, with the proposed $\gamma(t)$, the spikes of the DC link voltage and of the inductor current were smoothed (figs. 5b and 5c), while also respecting the converter capability during the transient (fig. 7).

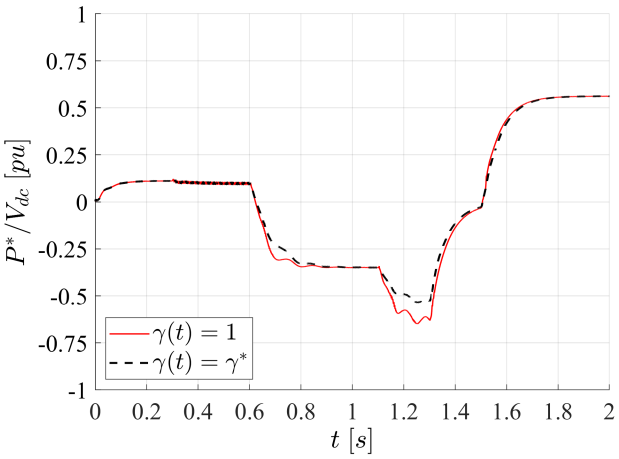

(a) Scheduling variable

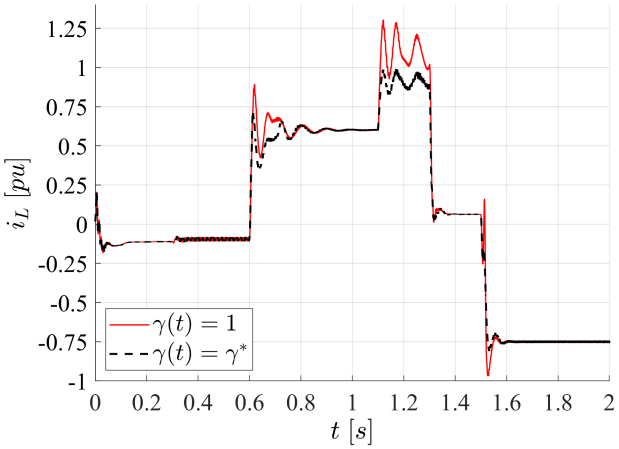

(b) Battery side inductor current

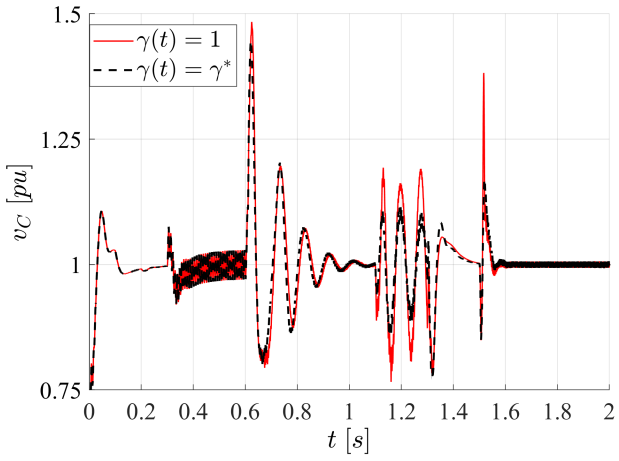

(c) DC link voltage

Fig. 5. DC/DC converter state variables (filtered measurements) for different γ values.

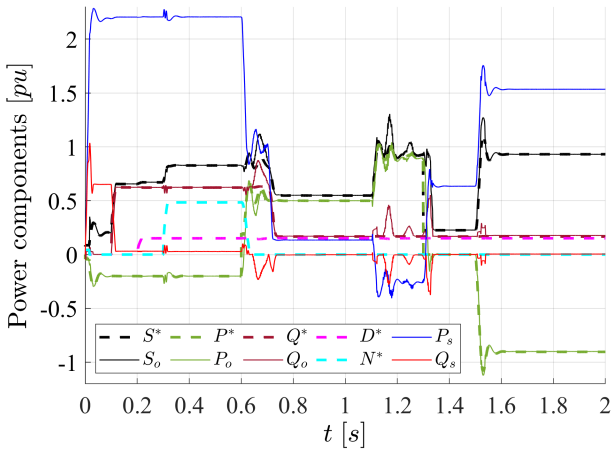

Fig. 6. Measured and reference power components at the DC/AC converter output for $\gamma(t) = 1$ (base power is S_r and due to this normalization grid power can be above 2 p.u.).

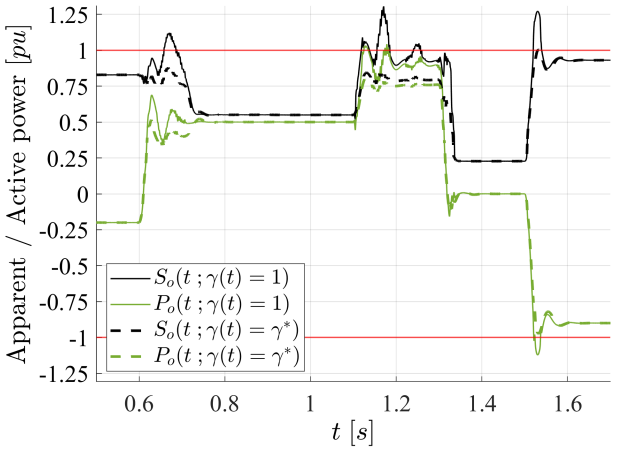

Fig. 7. Measured apparent and active power at the DC/AC converter output for different γ values.

TABLE IV
POWER QUALITY AND CPT INDICES.

Time [s]	λ_Q	λ_D	λ_U	λ	PF_{pcc}	*TDD [%]*
0.0	0.000	0.000	0.000	1.000	0.941	6.00
0.1	0.952	0.000	0.000	0.305	0.975	6.05
0.2	0.952	0.225	0.000	0.299	0.977	0.32
0.3	0.951	0.182	0.595	0.243	1.00	0.40

V. DISCUSSION AND CONCLUSIONS

Under the current trends in the offshore O&G sector for sustainable platform operation with higher reliance on RES, short-term energy storage solutions are expected to have an important role towards that direction. In this paper, the multiple benefits that can be achieved from a BESS and its dedicated converter, connected to an isolated offshore platform were demonstrated. A power management strategy was proposed that allowed the BESS to simultaneously follow the charging schedule (with negligible transient deviations), enhance the local power quality by providing reactive, harmonic and unbalance current compensation and attenuate the effects of the interactions between the DC and AC side converters, which are hard to model in advance. This strategy manipulated the allowable converter capacity such that the converter output power, even when sized based on the storage power rating, could respect the physical limitations also under severe disturbances. Due to its simple structure, the same algorithm could potentially be integrated with upper layer energy management systems, in order to dynamically reserve a portion of the converter's capacity, for various services, such as frequency support.

ACKNOWLEDGEMENTS

Project / research funded by VISTA - a basic research program in collaboration between The Norwegian Academy of Science and Letters, and Equinor.

This scientific paper was supported by the Onassis Foundation - Scholarship ID: F ZP 056-1/2019-2020.

This research was also partly funded under the program PETROMAKS2 of the Research Council of Norway, within the project "Smart Platform" (grant number 308735).

REFERENCES

[1] S. Settemsdal, L. Barstad, and W. Voss, "Hybrid power plants can help decarbonize offshore drilling rigs and vessels," p. 4.

[2] R. N. Fard and E. Tedeschi, "Integration of distributed energy resources into offshore and subsea grids," *CPSS Transactions on Power Electronics and Applications*, vol. 3, no. 1, pp. 36–45, Mar. 2018, conference Name: CPSS Transactions on Power Electronics and Applications.

[3] W. He, G. Jacobsen, T. Anderson, F. Olsen, T. D. Hanson, M. Korpås, T. Toftevaag, J. Eek, K. Uhlen, and E. Johansson, "The Potential of Integrating Wind Power with Offshore Oil and Gas Platforms," *Wind Engineering*, vol. 34, no. 2, pp. 125–137, Mar. 2010.

[4] S. Sanchez, E. Tedeschi, J. Silva, M. Jafar, and A. Marichalar, "Smart load management of water injection systems in offshore oil and gas platforms integrating wind power," *IET Renewable Power Generation*, vol. 11, no. 9, pp. 1153–1162, Jul. 2017.

[5] J. D. Macpherson, P. N. Jogi, and B. E. Vos, "Measurement of Mud Motor Rotation Rates using Drilling Dynamics," p. 10.

[6] M. G. Abidi, M. Ben Smida, M. Khalgui, Z. Li, and T. Qu, "Source Resizing and Improved Power Distribution for High Available Island Microgrid: A Case Study on a Tunisian Petroleum Platform," *IEEE Access*, vol. 7, pp. 22 856–22 871, 2019.

[7] D. Pavković, A. Sedić, and Z. Guzović, "Oil drilling rig diesel power-plant fuel efficiency improvement potentials through rule-based generator scheduling and utilization of battery energy storage system," *Energy Conversion and Management*, vol. 121, pp. 194–211, Aug. 2016.

[8] S. Chapaloglou, D. Varagnolo, and E. Tedeschi, "Techno-Economic Evaluation of the Sizing and Operation of Battery Storage for Isolated Oil and Gas Platforms with High Wind Power Penetration," in *IECON 2019 - 45th Annual Conference of the IEEE Industrial Electronics Society*, vol. 1, Oct. 2019, pp. 4587–4592, iSSN: 2577-1647.

[9] E. Alves, S. Sanchez, D. Brandao, and E. Tedeschi, "Smart Load Management with Energy Storage for Power Quality Enhancement in Wind-Powered Oil and Gas Applications," *Energies*, vol. 12, no. 15, p. 2985, Aug. 2019.

[10] J. Z. Tee, K. H. Tan, I. L. H. Lim, K. Zhou, and O. Anaya-Lara, "Integration of Offshore Wind with O G Platforms with an Energy Storage System," in *2019 IEEE PES Innovative Smart Grid Technologies Europe (ISGT-Europe)*, Sep. 2019, pp. 1–5, iSSN: null.

[11] J. Z. Tee, I. L. H. Lim, J. Yang, C. T. Choo, O. Anaya-Lara, and C. K. Chui, "Power System Stability of Offshore Wind with an Energy Storage to Electrify O G Platform," in *2020 IEEE REGION 10 CONFERENCE (TENCON)*, Nov. 2020, pp. 146–151, iSSN: 2159-3450.

[12] M. Alhaddad, "Mitigation of Harmonic Problems of an Offshore Drilling Jack-Up Rig Power System," in *Abu Dhabi International Petroleum Exhibition & Conference*. Abu Dhabi, UAE: Society of Petroleum Engineers, 2018.

[13] V. Verma, B. Singh, A. Chandra, and K. Al-Haddad, "Power Conditioner for Variable-Frequency Drives in Offshore Oil Fields," *IEEE Transactions on Industry Applications*, vol. 46, no. 2, pp. 731–739, Mar. 2010, conference Name: IEEE Transactions on Industry Applications.

[14] E. Chatzinikolaou and D. J. Rogers, "A Comparison of Grid-Connected Battery Energy Storage System Designs," *IEEE Trans. Power Electron.*, vol. 32, no. 9, pp. 6913–6923, Sep. 2017.

[15] L. A. Vitoi, D. I. Brandao, and E. Tedeschi, "Power quality enhancement by SiC Active Power Filters in Oil and Gas Platforms," in *2019 IEEE Energy Conversion Congress and Exposition (ECCE)*. Baltimore, MD, USA: IEEE, Sep. 2019, pp. 4299–4304.

[16] H. K. M. Paredes, F. P. Marafão, D. I. Brandão, and A. Costabeber, "Multi-task control strategy for grid-tied inverters based on conservative power theory," *IET Renewable Power Generation*, vol. 9, no. 2, pp. 154–165, Mar. 2015.

[17] P. Tenti, H. K. M. Paredes, and P. Mattavelli, "Conservative Power Theory, a Framework to Approach Control and Accountability Issues in Smart Microgrids," *IEEE Transactions on Power Electronics*, vol. 26, no. 3, pp. 664–673, Mar. 2011, conference Name: IEEE Transactions on Power Electronics.

[18] A. Reznik, M. G. Simoes, A. Al-Durra, and S. M. Muyeen, "LCL Filter Design and Performance Analysis for Grid-Interconnected Systems," *IEEE Trans. on Ind. Applicat.*, vol. 50, no. 2, pp. 1225–1232, Mar. 2014.

[19] M. Liserre, F. Blaabjerg, and S. Hansen, "Design and control of an LCL-filter-based three-phase active rectifier," *IEEE Transactions on Industry Applications*, vol. 41, no. 5, pp. 1281–1291, Sep. 2005, conference Name: IEEE Transactions on Industry Applications.

[20] E. Tedeschi, P. Tenti, P. Mattavelli, and D. Trombetti, "Cooperative control of electronic power processors in micro-grids," in *2009 Brazilian Power Electronics Conference*, Sep. 2009, pp. 1–8, iSSN: 2165-0454.

[21] L. S. Xavier, W. C. S. Amorim, A. F. Cupertino, V. F. Mendes, W. C. do Boaventura, and H. A. Pereira, "Power converters for battery energy storage systems connected to medium voltage systems: a comprehensive review," *BMC Energy*, vol. 1, no. 1, p. 7, Dec. 2019.

[22] P. H. I. Hayashi and L. Matakas, "Decoupled stationary ABC frame current control of three-phase four-leg four-wire converters," in *2017 Brazilian Power Electronics Conference (COBEP)*. Juiz de Fora: IEEE, Nov. 2017, pp. 1–6.

[23] S. Buso and P. Mattavelli, *Digital Control in Power Electronics*, Jan. 2006, vol. 1.

[24] "IEEE Recommended Practice and Requirements for Harmonic Control in Electric Power Systems," *IEEE Std 519-2014 (Revision of IEEE Std 519-1992)*, pp. 1–29, Jun. 2014, conference Name: IEEE Std 519-2014 (Revision of IEEE Std 519-1992).